Comparative investigation of Schottky barrier height of Ni/n-type Ge and Ni/n-type GeSn

Li Sian Jheng, Hui Li, Chiao Chang, Hung Hsiang Cheng, and Liang Chen Li

Citation: AIP Advances **7**, 095324 (2017); doi: 10.1063/1.4997348
View online: http://dx.doi.org/10.1063/1.4997348
View Table of Contents: http://aip.scitation.org/toc/adv/7/9
Published by the American Institute of Physics

Articles you may be interested in

Room-temperature 2-μm GeSn P-I-N homojunction light-emitting diode for inplane coupling to group-IV waveguides
Applied Physics Letters **111**, 141105 (2017); 10.1063/1.4999395

Raman spectral shift versus strain and composition in GeSn layers with 6%–15% Sn content
Applied Physics Letters **110**, 112101 (2017); 10.1063/1.4978512

Silicon-immersed terahertz plasmonic structures
Applied Physics Letters **110**, 151105 (2017); 10.1063/1.4980018

Optically pumped GeSn micro-disks with 16% Sn lasing at 3.1 μm up to 180 K
Applied Physics Letters **111**, 092101 (2017); 10.1063/1.5000353

Investigation of optical transitions in a SiGeSn/GeSn/SiGeSn single quantum well structure
Journal of Applied Physics **122**, 123102 (2017); 10.1063/1.4986341

Comparative investigation of Schottky barrier height of Ni/n-type Ge and Ni/n-type GeSn

Li Sian Jheng,[1] Hui Li,[1] Chiao Chang,[1] Hung Hsiang Cheng,[1,a] and Liang Chen Li[2]

[1]*Center for Condensed Matter Sciences and Graduate Institute of Electronics Engineering, National Taiwan University, Taipei 106, Taiwan, R. O. C.*

[2]*Center for Nano Science and Technology, National Chiao Tung University, Hsinchu 300, Taiwan, R.O.C.*

(Received 24 July 2017; accepted 21 September 2017; published online 29 September 2017)

We report an investigation of the Schottky barrier height (SBH) of Ni/n-type Ge and Ni/n-type GeSn films that is annealed at a wide range of temperatures. Both voltage- and temperature-dependent current–voltage (I–V) measurements are performed. From the analysis of these nonlinear I–V traces, the SBH is found and the results shows that the SBH of Ni/n-type GeSn (a) is smaller than that of Ni/n-type Ge and (b) decreases with the Sn content of the surface GeSn layer associated with the thermal annealing. By modeling the composition- and strain-dependent energy bandgap (E_g), the relationship between the SBH and E_g is established and it is found that SBH/E_g ~0.8. These results suggest that the GeSn film could serve as an interfacial layer for the reduction of the SBH in Ge-based electronic devices that are desirable for applications. © *2017 Author(s). All article content, except where otherwise noted, is licensed under a Creative Commons Attribution (CC BY) license (http://creativecommons.org/licenses/by/4.0/).* https://doi.org/10.1063/1.4997348

The group-IV materials of Ge and GeSn have attracted attention for their potential applications in high-speed electronic devices.[1–3] The incorporation of Sn modulates the energy profile of the host material Ge[4,5] and, above a certain Sn content, the energy profile of the alloy transforms from an indirect to direct bandgap material, which is desirable for application in photonic devices.[6–8] In the processing of these films into devices, a metal/semiconductor electrical contact is fabricated. Here, we report an investigation of the Schottky barrier height (SBH) of Ni/n-type Ge and Ni/n-type GeSn films that is annealed at a range of temperatures from 350 to 420 °C. Current–voltage (I–V) measurements are performed and the results suggest that these traces nonlinearly represent a potential barrier at the Ni/n-type Ge and Ni/n-type GeSn interface. From the analysis, the SBH is found to decrease as the annealing temperature increases up to 390 °C and remain almost constant as the annealing temperature further increases. The decrease in the SBH is attributed to the change in Sn content at the surface of the GeSn layer, as measured by X-ray photoelectron spectroscopy (XPS), caused by the thermal annealing. By modeling the composition- and strain-dependent energy bandgap (E_g) of the GeSn alloy, the relationship between the SBH and E_g is established and it is found that SBH/E_g ~0.8.

The sample is grown on an n-type Ge wafer with a resistivity of 1 Ω·cm by using solid-source molecular beam epitaxy. The sample consists of (a) a 4.5-nm-thick Ge layers and (b) a 160-nm-thick GeSn layer. Both layers are n-doped. The thickness of the layers is measured by transmission electron microscopy. The doping concentration of the layers is characterized by secondary ion mass spectrometry measurements and the carrier concentration was found to be 2×10^{18} cm^{-3}, which is approximately equivalent to the doping concentration of the Ge wafer. High-resolution X-ray diffraction measurements are performed in a (004) scan and a (224) reciprocal space map is employed

[a]Corresponding author: hhcheng@ntu.edu.tw

 © Author(s) 2017

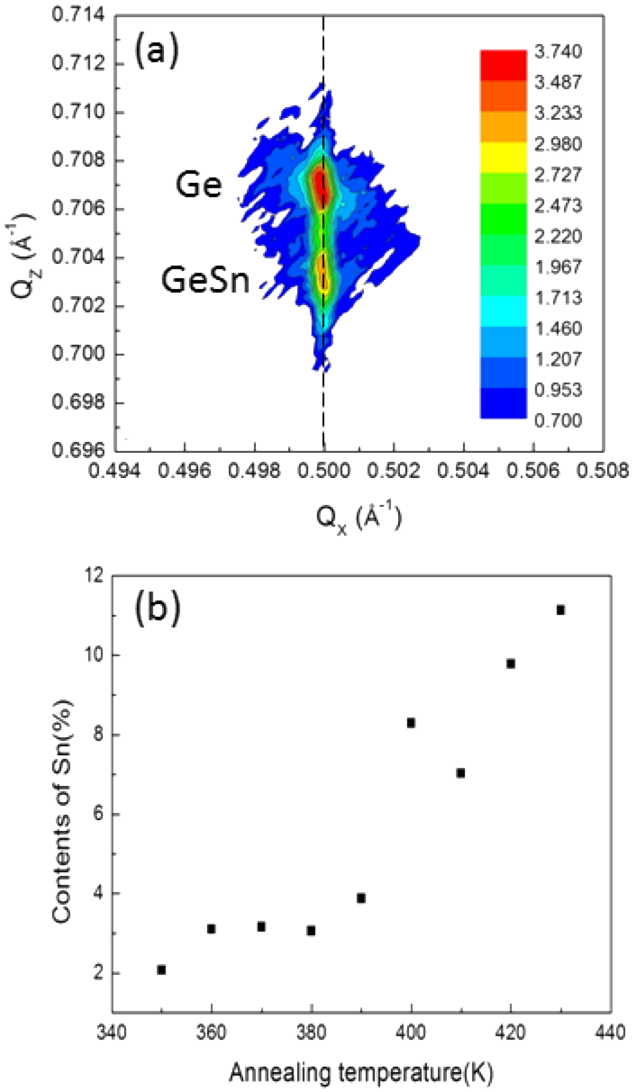

FIG. 1. (a) The (224) reciprocal space mapping of the as-grown sample. (b) Sn contents plotted as a function of annealing temperature.

to probe the Sn content and the status of the strain in the GeSn layer. The (224) reciprocal space mapping of the sample is plotted in Figure 1(a). In the plot, the x-axis and y-axis scale with the in-plane ($a_{\parallel}$) and out-of-plane ($a_{\perp}$) lattice constants $Q_x = \sqrt{8}/a_{\parallel}$ and $Q_z = 4/a_{\perp}$. The plot shows that the diffraction peaks of the GeSn layer and the Ge substrate are located at the same Q_x as marked by the dashed line, indicating that the GeSn layer is compressively strained to the lattice structure of the Ge wafer (i.e., fully strained). From the analysis of the peak position of the X-ray traces and by comparing with the composition-dependent lattice constant of bulk GeSn, the composition is first established and the Sn content is found to be 2.1%. With this lattice constant, the in-plane strains, ε_{xx} and ε_{yy}, can be calculated by $\varepsilon_{xx} = \varepsilon_{yy} = (a_{\mathrm{Ge}} - a_{\mathrm{GeSn}})/a_{\mathrm{GeSn}}$, where a_{Ge} and a_{GeSn} are the relaxed lattice constants of Ge and $Ge_{1-x}Sn_x$, respectively, while the strain in the growth direction can be evaluated by $\varepsilon_{zz} = -2C_{12}/C_{11}\varepsilon_{xx}$, where C_{11} and C_{12} are elastic constants. By taking a linear interpolation between Ge and α-Sn for these parameters for the $Ge_{0.979}Sn_{0.021}$ alloy, the strain of the layer is found to be ε_{xx}=0.3% and ε_{zz}=0.2%.

For the electrical current–voltage (I–V) measurements, metal contacts are fabricated on the bottom and top of the sample. Two types of samples are fabricated. The first type is the GeSn

sample described above, while the second type is the Ge wafer used in this study. On the bottom of the sample, AuSb alloy with a Sb composition of 1% is used and deposited by thermal evaporation followed by rapid thermal annealing at 380 °C to form an Ohmic contact. After the fabrication of the bottom contact, the sample with the GeSn film is annealed at a temperature range between 350 and 420 °C at a temperature interval of 10°C. After annealing, Ni is deposited on the top of the samples followed by rapid thermal annealing at 350 °C to form a contact with a low specific contact resistivity. In performing the thermal treatment, we like to point out, the thermal annealing drives the Sn atoms to the surface of the GeSn layer, forming a thin GeSn layer with a Sn composition larger than the underlying GeSn film, is due to the low melting point of Sn. (In driving the Sn to the surface layer, in reference 9, it has been demonstrated that above the annealing temperature of 390 °C, the GeSn film starts to relax, accompanied by the misfit dislocation developed at the GeSn/Ge interface.) The Sn composition in the surface layer is measured by XPS with a probing depth of around 10 nm. The result shows that the Sn composition increases from 2.1% for the sample without annealing to 12% for the sample annealed at 390 °C, as plotted in Figure 1(b).

The I–V trace measured under a forward bias for the GeSn film sample is plotted in Figure 2. These traces exhibit a nonlinear behavior reflecting the potential barrier formed at the interface between the Ni and GeSn (Schottky potential). The characteristics of these traces can be categorized into two groups: at a fixed voltage, (a) for the samples with annealing temperatures below 390 °C, the current decreases with annealing temperature; (b) for samples with annealing temperatures above 390 °C, the current increases and the magnitude of the current is roughly equivalent to that of the as-grown sample. The increase in current is attributed to the misfit dislocation generated at high annealing temperatures, as discussed above.

These I–V traces are analyzed based on the thermionic emission model to determine the SBH. The current is

$$I = AA^{*}T^{2}\exp\left(\frac{-q\varphi_b}{kT}\right)\exp\left(\frac{qV_d}{nkT} - 1\right) \quad (1)$$

where A* and T are the Richardson constant and temperature in which the measurement was performed, respectively. The first factor accounts for the SBH(φ_b) and, in the conventional approach, its value is determined by the difference of the work function of the metal and electron affinity of the semiconductor. The second factor is the voltage drop (V_d) across the schottky diode and n is the non-ideality factor. Following the methodology developed in reference 10, the SBH is analyzed. First, the non-ideality factor is deduced by rearranging and differentiating Eq. (1). With this value, the SBH can then be determined from the y-axis intercept of $V - n\frac{KT}{q}\ln\left(\frac{I}{AA^{*}T^{2}}\right)$ vs. $RI + n\varphi_b$. The resulting SBH is plotted in Figure 3.

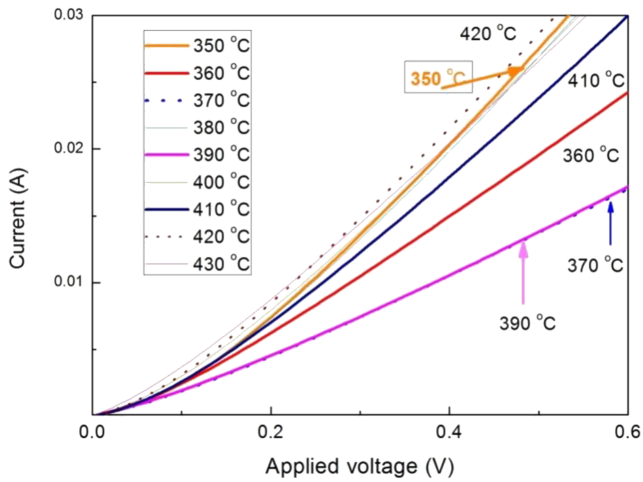

FIG. 2. I–V traces of the GeSn sample measured under forward bias at different annealing temperatures.

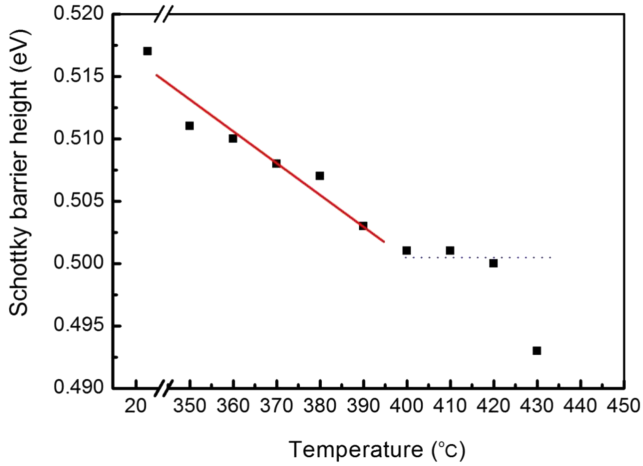

FIG. 3. SBH plotted as a function of annealing temperature.

It shows that for the Ge wafer, the SBH is 0.55eV, which is consistent with that reported in the literature.[11–14] For the GeSn film, the SBH decreases as the annealing temperature increases up to an annealing temperature of 390 °C, as indicated by the solid line. The SBH remains almost constant the annealing temperature further increases, as indicated by the dashed line. In the later discussion, we will focus on the results of those samples with annealing temperatures below 390 °C as defects start to form with annealing temperatures above 390 °C.

The SBH found in the Ni/GeSn system is smaller than that in the Ni/n-type Ge. For the Ni/n-type Ge system, as suggested by the experimental results, the Fermi level of Ni matches with the energy level of about 0.11eV above the valence band (VB) edge, where, in terms of its indirect bandgap (E_g), SBH is 0.824E_g (the E_g of bulk Ge is 0.664eV).[13,14] Therefore, as the value of the SBH depends on the bandgap, we first discuss the composition- and strain-dependent bandgap of the GeSn alloy. As the electric transport is dominated by the lowest band, we focus on the relaxed indirect band (L-band), of which the bandgap is

$$E(\mathrm{Ge}_{1-x}\mathrm{Sn}_x) = E_{\mathrm{Ge}}\,(1-x) + E_{\mathrm{Sn}}x - bx\,(1-x) \tag{2}$$

where E_{Ge} and E_{Sn} are the Ge and Sn bandgaps at the L-valleys measured from the top of the VB for Ge and Sn, respectively. b= 0.89 is bowing parameter.[15] The strain in the GeSn layer shifts both the conduction band (CB) edge and VB edge. The amount of energy shift is $\Delta E_c = a_c(\varepsilon_{xx} + \varepsilon_{yy} + \varepsilon_{zz})$ for the CB and $\Delta E_v = b_v(\varepsilon_{xx} + \varepsilon_{yy} + \varepsilon_{zz}) + b_s(\varepsilon_{zz} - \varepsilon_{xx})$ for the VB, where a_c is the CB deformation

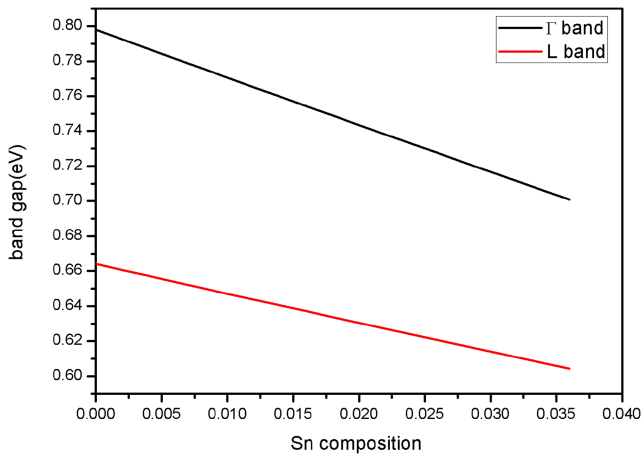

FIG. 4. The bandgaps of the GeSn alloy plot as a function of Sn content measured by the XPS.

TABLE I. Summary of the measured SBH and bandgap energy of Ge and GeSn samples annealed below 390 °C.

	Ge	Sn=2.4	Sn=2.6	Sn=2.5	Sn=3.4
SBH (eV)	0.55	0.517	0.511	0.51	0.507
Eg (eV)	0.664	0.624	0.62	0.621	0.607
SBH/Eg	0.828	0.828	0.824	0.821	0.835

potential, and b_v and b_s are the VB deformation potentials. By taking a linear interpolation between Ge and Sn for the deformation potential of the GeSn alloys and the measured strain discussed above, the bandgaps of the GeSn alloy with Sn content measured by the XPS are calculated. The result is plotted in Figure 4 and shows that the bandgap decreases with Sn content. To make quantitative comparison, the measured SBH and calculated bandgap are tabulated in Table I. It shows that the SBH decreases as the bandgap of the GeSn surface layer decreases. The ratio of the SBH and E_g of the GeSn samples lies between 0.821 and 0.835. This indicates that the Fermi energy of Ni matches with an energy level (~0.17 E_g) above the VB edge, similar to that of Ni/n-type Ge.

In summary, we report the investigation of the SBH of Ni/n-type Ge and Ni/n-type GeSn systems. We demonstrate that the SBH decreases as the bandgap of the GeSn surface layer at the interface between the metal and GeSn film decreases. From the analysis, the SBH is a factor of about 0.8 of its bandgap. In demonstrating these results, we should point out that for Ge-based electronic devices, which have attracted much attention in the recent development of high-mobility electronic devices, a thin GeSn layer deposited on the Ge layer could serve as an interfacial layer for the electrical contact on Ge-based electronic devices. This could provide a small SBH for devices that are desired in applications.

ACKNOWLEDGMENTS

The authors would like to thank the Ministry of Science and Technology Taiwan for its financial support under Grant No. 104-2623-E-002-007-D and 104-2112-M-002-010-MY3, the MOST-2622-E-002-031, and the U.S. Army Asian Office of Aerospace Research & Development under the contract No. FA2386-14-1-4073.

[1] C. Claeys and E. Simoen, *Germanium-Based Technologies: From Materials to Devices* (Elsevier, Amsterdam, 2007), pp. 363–379.
[2] R. Pillarisetty, "Academic and industry research progress in germanium nanodevices," Nature **479**(7373), 324–328 (2011).
[3] S. Gupta, R. Chen, B. Magyari-Kope, H. Lin, B. Yang, A. Nainani, Y. Nishi, J. S. Harris, and K. C. Saraswat, "GeSn technology: Extending the Ge electronics roadmap," Proc. IEEE Int. Electron Devices Meeting, pp. 398–401, 2011-Dec.
[4] R. Chen, H. Lin, Y. Huo, C. Hitzman, T. I. Kamins, and J. S. Harris, Appl. Phys. Lett. **99**, 181125 (2011).
[5] S. Gupta, B. Magyari-Köpe, Y. Nishi, and K. C. Saraswat, Journal of Applied Physics **113**, 073707 (2013).
[6] H. H. Tseng, K. Y. Wu, H. Li, V. Mashanov, H. H. Cheng, G. Sun, and R. A. Soref, Appl. Phys. Lett. **102**, 182106 (2013).
[7] M. Oehme, K. Kostecki, T. Arguirov, G. Mussler, K. Ye, M. Gollhofer, M. Schmid, M. Kaschel, R. Körner, M. Kittler, D. Buca, E. Kasper, and J. Schulze, IEEE Photonics Technol. Lett. **26**, 187 (2014).
[8] J. Zheng, S. Wang, Z. Liu, H. Cong, C. Xue, C. Li, Y. Zuo, B. Cheng, and Q. Wang, Appl. Phys. Lett. **108**, 033503 (2016).
[9] H. Li, Y. X. Cui, K. Y. Wu, W. K. Tseng, H. H. Cheng, and H. Chen, Appl. Phys. Lett. **102**, 251907 (2013).
[10] S. K. Cheung and N. W. Cheung, Appl. Phys. Lett. **49**, 85 (1986).
[11] Y. Zhou, M. Ogawa, X. Han, and K. L. Wang, Appl. Phys. Lett. **93**, 202105 (2008).
[12] M. K. Husian, X. V. Li, and C. H. de Groot, IEEE Transactions on Electron Device **56**(3), 499–504 (2009).
[13] T. Nishimura, K. Kita, and A. Toriumi, Appl. Phys. Lett. **91**, 123123 (2007).
[14] A. Dimoulas, P. Tsipas, A. Sotiropoulos, and E. K. Evangelou, Appl. Phys. Lett. **89**, 252110 (2006).
[15] W.-J. Yin, X.-G. Gong, and Su-H. Wei, Phys. Rev. B **78**, 161203(R) (2008).